JCI insight

Impact of genetic factors on antioxidant rescue of maternal diabetes-associated congenital heart disease

Talita Z. Choudhury, … , Ming-Tao Zhao, Vidu Garg

JCI Insight. 2024. https://doi.org/10.1172/jci.insight.183516.

Research In-Press Preview Cardiology Development

Congenital heart disease (CHD) affects ~1% of live births. Although genetic and environmental etiologic contributors have been identified, the majority of CHD lacks a definitive cause, suggesting the role of gene-environment interactions (GxE) in disease pathogenesis. Maternal diabetes mellitus (matDM) is among the most prevalent environmental risk factors for CHD. However, there is a substantial knowledge gap in understanding how matDM acts upon susceptible genetic backgrounds to increase disease expressivity. Previously, we reported a GxE between Notch1 haploinsufficiency and matDM leading to increased CHD penetrance. Here, we demonstrate a cell lineage specific effect of *Notch1* haploinsufficiency in matDM-exposed embryos, implicating endothelial/endocardial derived tissues in the developing heart. We report impaired atrioventricular cushion morphogenesis in matDM exposed *Notch1*$^{+/-}$ animals and show a synergistic effect of *NOTCH1* haploinsufficiency and oxidative stress in dysregulation of gene regulatory networks critical for endocardial cushion morphogenesis in vitro. Mitigation of matDM-associated oxidative stress via *SOD1* overexpression did not rescue CHD in *Notch1* haploinsufficient mice compared to wildtype littermates. Our results show the combinatorial interaction of matDM-associated oxidative stress and a genetic predisposition, *Notch1* haploinsufficiency, on cardiac development, supporting a GxE model for CHD etiology and suggesting that antioxidant strategies maybe ineffective in genetically-susceptible individuals.

Title: Impact of genetic factors on antioxidant rescue of maternal diabetes-associated congenital heart disease

Authors: Talita Z. Choudhury[1,2], Sarah C. Greskovich[1], Holly B. Girard[1], Anupama S. Rao[1], Yogesh Budhathoki[2], Emily M. Cameron[1], Sara Conroy[3,4], Deqiang Li[1,4], Ming-Tao Zhao[1,4], Vidu Garg[1,4,5]

[1]Center for Cardiovascular Research, Abigail Wexner Research Institute, and The Heart Center, Nationwide Children's Hospital, Columbus, Ohio, USA

[2]Molecular, Cellular, Developmental Biology Graduate Program, The Ohio State University, Columbus, Ohio, USA

[3]Center for Perinatal Research, Abigail Wexner Research Institute, Nationwide Children's Hospital, Columbus, Ohio, USA

[4]Department of Pediatrics, The Ohio State University, Columbus, Ohio, USA

[5]Department of Molecular Genetics, The Ohio State University, Columbus, Ohio, USA

Conflict of interest: The authors have declared that no conflict of interest exists

Correspondence:

Vidu Garg M.D., Center for Cardiovascular Research and The Heart Center, Nationwide Children's Hospital, Room WB4275 Columbus, OH 43205. Phone: 614-355-5710, Fax: 614-355-5725. Email: vidu.garg@nationwidechildrens.org

ORCID Identifier: 0000-0002-3778-5927

Word count: 8813

Abstract

Congenital heart disease (CHD) affects ~1% of live births. Although genetic and environmental etiologic contributors have been identified, the majority of CHD lacks a definitive cause, suggesting the role of gene-environment interactions (GxE) in disease pathogenesis. Maternal diabetes mellitus (matDM) is among the most prevalent environmental risk factors for CHD. However, there is a substantial knowledge gap in understanding how matDM acts upon susceptible genetic backgrounds to increase disease expressivity. Previously, we reported a GxE between *Notch1* haploinsufficiency and matDM leading to increased CHD penetrance. Here, we demonstrate a cell lineage specific effect of *Notch1* haploinsufficiency in matDM-exposed embryos, implicating endothelial/endocardial derived tissues in the developing heart. We report impaired atrioventricular cushion morphogenesis in matDM exposed *Notch1*$^{+/-}$ animals and show a synergistic effect of *NOTCH1* haploinsufficiency and oxidative stress in dysregulation of gene regulatory networks critical for endocardial cushion morphogenesis *in vitro*. Mitigation of matDM-associated oxidative stress via *SOD1* overexpression did not rescue CHD in *Notch1* haploinsufficient mice compared to wildtype littermates. Our results show the combinatorial interaction of matDM-associated oxidative stress and a genetic predisposition, *Notch1* haploinsufficiency, on cardiac development, supporting a GxE model for CHD etiology and suggesting that antioxidant strategies maybe ineffective in genetically-susceptible individuals.

Key words: maternal diabetes; congenital heart disease; oxidative stress, Notch1, endocardial cushions, endothelial cells

Introduction

Congenital heart disease (CHD) affects ~1% of live births and is the leading cause of birth-defect related infant mortality (1). Although high-throughput genome sequencing technologies have made remarkable advances in uncovering genetic etiologies for CHD, the underlying cause for more than half of CHD cases is still unknown (2-5). A subset of these cases have long been proposed to be the combinatorial effect of genetic predisposition and environmental influences, resulting in complex inheritance patterns and variable CHD expressivity (6,7). Among environmental contributors, maternal pre-gestational diabetes mellitus is a highly prevalent and well-established risk factor for CHD, increasing the risk of having an infant with CHD by 3-5-fold (8-13). The influence of maternal diabetes mellitus (matDM) on cardiac development has been studied in animal models, shedding light on key cellular and molecular pathways particularly vulnerable to this environmental milieu (14). Recently, matDM has been shown to have cell lineage-specific effects during cardiac morphogenesis, specifically affecting the second heart field (SHF) and neural crest lineages to disrupt cardiomyocyte differentiation and anterior-posterior specification (15,16). The incidence of CHD in a pregnancy complicated by pre-gestational diabetes mellitus has remained elevated even with substantial advancements in prenatal care suggesting that matDM may cause CHD by acting on susceptible genetic backgrounds, i.e., gene-environment interaction (GxE) etiology. However, the cellular and molecular basis for GxE in CHD as postulated in the multifactorial hypothesis for CHD remain limited (6,17,18).

Cardiac development is a dynamic process with tight spatiotemporal regulation of several multipotent cardiac cell lineages (19,20). Endothelial-to-mesenchymal transition (EndMT) is a crucial process that occurs early in heart development wherein endocardial cells lining the atrioventricular canal (AVC) and developing outflow tract (OFT) detach from the monolayer and migrate into the preformed cardiac jelly to form endocardial cushions (21-23). Subsequent remodeling of the endocardial cushions at the AVC leads to the formation of the atrioventricular valve leaflets, atrioventricular septum, and membranous portion of the ventricular septum (24,25). At the OFT, endocardial cushions receive additional contributions from the migrating cardiac neural crest cells to form the semilunar valves and aorticopulmonary septum (26). Although matDM is associated with a spectrum of CHD phenotypes, the most commonly observed include septal and conotruncal (involving OFT and great vessels) heart defects, suggesting EndMT and endocardial cushion morphogenesis are particularly susceptible to disruption by the abnormal diabetic environment (10,11). This is supported by several published studies in animal models showing dysregulation of key EndMT signaling pathways in embryonic hearts exposed to matDM including BMP, TGFβ, and Notch signaling (27-31). Additionally, oxidative stress is a hallmark of diabetic embryopathy, and impaired redox signaling has been implicated in dysregulation of several cardiac developmental pathways suggesting that matDM-associated oxidative stress may be culpable for the elevated risk of CHD (31,32).

Previously, we found matDM interacts with *Notch1* haploinsufficiency in mice to increase the incidence of membranous ventricular septal defects (VSD), reporting a GxE between *Notch1* and matDM (27). Pathogenic *NOTCH1* variants are associated with a

spectrum of CHD in humans and Notch signaling is known to interact with other signaling pathways such as BMP and TGFβ to facilitate EndMT in the developing heart (33-38). To better characterize the *Notch1*-matDM GxE and place it in the context of cardiac development, we hypothesized that matDM and *Notch1* haploinsufficiency functionally converge to disrupt endocardial cushion morphogenesis and EndMT to increase the risk of CHD.

In this study, we demonstrate that matDM and *Notch1* haploinsufficiency interact within the developing endothelial/endocardial and endocardial-derived mesenchyme to increase the incidence of membranous VSD. We report abnormal AV cushion morphogenesis in matDM-exposed *Notch1*$^{+/-}$ embryonic hearts compared to non-diabetic controls. In a human induced pluripotent stem cell (iPSC)-based *in vitro* model, we show that *NOTCH1* haploinsufficiency sensitizes endothelial cells to the effects of oxidative stress and disrupts a network of genes and biological processes underlying EndMT and endocardial cushion morphogenesis. Consistent with this, we find matDM-exposed *Notch1*$^{+/-}$ embryos are insensitive to antioxidant based therapeutic strategy, despite rescue of VSD observed in matDM-exposed WT littermates. Overall, the results from this study elucidate mechanisms by which matDM interacts with a genetic susceptibility, i.e., *Notch1* haploinsufficiency, to bring about cell lineage-specific effects and increase penetrance of CHD. This work serves as experimental proof supporting a multifactorial etiology for CHD, underscoring the need to identify novel genetic modifiers that act in conjunction with environmental teratogens to increase the incidence of CHD and shows the variability in phenotypic rescue with antioxidant therapies in a genetically-susceptible background.

Results

Gene-environment interaction between endothelial Notch1 haploinsufficiency and maternal diabetes mellitus causes congenital heart defects

Previously, we identified a novel GxE between *Notch1* haploinsufficiency and matDM in mice, wherein *Notch1*$^{+/-}$ embryos exposed to matDM had significantly higher incidence of VSD compared to WT littermates at embryonic day (E)13.5 (27). We first sought to determine if this GxE is evident at a later developmental stage in mice. For this, we generated STZ-induced diabetic WT females for timed-mating with non-diabetic *Notch1*$^{+/-}$ males. Analysis of matDM-exposed embryos at E14.5 (n=3 litters) confirmed previously reported GxE resulting in significantly higher incidence of membranous VSD in *Notch1*$^{+/-}$ (10/14, 71%) embryos compared to WT littermates (1/10, 10%, Fisher's exact test p value = 0.005) (Supplementary figure 1A-C).

The expression pattern of activated NOTCH1 in the developing heart has been well characterized, being highly expressed within endocardial and endocardial-derived mesenchymal cells which form the endocardial cushions at the AV canal and OFT (39,40). Subsequently, we sought to determine if endothelial-specific *Notch1* haploinsufficiency is sufficient to sensitize the effects of matDM on cardiac development. For this experiment, STZ-induced diabetic and non-diabetic *Notch1*$^{fl/fl}$ females were bred with non-diabetic *Tie2-Cre*$^{+}$ males to generate control and matDM-exposed *Notch1*$^{fl/wt}$*;Tie2-Cre*$^{+}$ embryos, which are conditionally heterozygous for *Notch1* in all endothelial cells including endocardial cells and their derived tissues in the heart (Figure 1A). While no VSD was found in non-diabetic *Notch1*$^{fl/wt}$*;Tie2-Cre*$^{+}$ or *Notch1*$^{fl/wt}$

littermates, we found a significantly higher incidence of membranous VSD in E14.5 matDM-exposed *Notch1*$^{fl/wt}$*;Tie2-Cre*$^{+}$ embryos (7/17, 41%) compared to non-*Cre*$^{+}$ littermates (3/31, 9.7%, Fisher's exact test p value = 0.022) (Figure 1B,C). To account for variability across multiple matDM-exposed litters (n=6), we used a general linear mixed model and included litter as the random effect and the probability of VSD for *Notch1*$^{fl/wt}$*;Tie2-Cre*$^{+}$ was found to be higher compared to *Notch1*$^{fl/wt}$ (p value = 0.06, see Supporting Data Values) (41). While this is slightly higher than the traditional 0.05 cut point, this still small p-value provides evidence that the data are not compatible with the null hypothesis (42). We also noted that the incidence of VSD in matDM-exposed *Notch1*$^{fl/wt}$*;Tie2-Cre*$^{+}$ (41%) was found to be lower than the incidence observed in matDM-exposed *Notch1*$^{+/-}$ (71%). We attribute this difference to potential roles of *Notch1* haploinsufficiency in non-endothelial derived cells of the heart in the GxE with matDM or this variability may be due to incomplete deletion of *Notch1* in all endothelial cells. Overall, these results suggest that the observed GxE between *Notch1* haploinsufficiency and matDM can act within the developing endothelium including the endocardium and endocardial-derived cells to impair cardiac morphogenesis, particularly ventricular septation.

Notch1 haploinsufficiency exacerbates the effects of maternal diabetes mellitus on atrioventricular cushion development

During cardiac development, endocardial cells undergo EndMT to form endocardial cushions at the AVC and OFT. Subsequent remodeling of the proximal OFT and AV cushions give rise to the atrioventricular septal complex which includes the mitral

and tricuspid valve leaflets and the membranous ventricular septum (24,25,43). Here, we sought to determine if interaction between *Notch1* haploinsufficiency and matDM impairs endocardial cushion morphogenesis at the OFT and AV canal. As Notch signaling is known to regulate EndMT during endocardial cushion development, we utilized the *Rosa26*$^{mT/mG}$ locus to trace endothelial cells that have undergone EndMT in endocardial cushions of matDM-exposed *Notch1*$^{+/-}$ embryos compared to non-diabetic controls. We analyzed histological sections of OFT and AV cushions at E11.5; volumetric analysis using 3D reconstruction of serial histological sections revealed matDM-exposed *Notch1*$^{+/-}$ hearts had significantly smaller AV cushion size compared to non-diabetic *Notch1*$^{+/-}$ and non-diabetic WT hearts (Figure 2A,B). On the other hand, matDM-exposed WT did not show a statistically significant difference in AV cushion size compared to non-diabetic controls. We found no significant difference in OFT cushion size across the four groups, suggesting that this GxE affects AV cushion morphogenesis to contribute to membranous VSD (Supplemental figure 2A,B). Upon examination of GFP+ EndMT derived cells within the AV cushions, GFP+ cells appeared more compacted within the AV cushion of matDM-exposed *Notch1*$^{+/-}$ hearts, which was likely due to the smaller AV cushion size (Figure 2C). This was quantified by counting the number of GFP+ cell nuclei within the AV cushion and a statistically significant increase in cell density was noted between matDM-exposed *Notch1*$^{+/-}$ embryos compared to non-diabetic *Notch1*$^{+/-}$ control (Figure 2D). Again, this effect is not observed in the matDM-exposed WT littermates and we noted a high degree of variability in this group, possibly due to the low penetrance of disease in matDM-exposed WT embryos. These results show that the overall size of the AV cushion is significantly smaller in the matDM-exposed *Notch1*$^{+/-}$ compared to non-diabetic

controls, causing EndMT derived cells to become more densely packed within the AV cushion.

The deposition and distribution of extracellular matrix components (ECM) including sulfated proteoglycans such as hyaluronic acid and versican are crucial for endocardial cushion formation and remodeling into the AV valvuloseptal complex, a process highly regulated by both endocardial and myocardial signaling adjacent to the AV cushion (44-46). Alcian blue staining of WT and *Notch1*$^{+/-}$ embryos of diabetic and non-diabetic dams at E11.5 showed reduced proteoglycan deposition in matDM-exposed *Notch1*$^{+/-}$ AV cushion compared to non-diabetic control while matDM-exposed WT did not show a difference compared to non-diabetic controls (Figure 3A, C). During AV cushion development, full-length versican undergoes proteolytic cleavage by the action of matrix metalloproteinases MMP2 and ADAMTS1 (47). Similarly, expression of cleaved versican, labeled by an antibody against neo-epitope DPEAAE, was significantly decreased in the matDM-exposed *Notch1*$^{+/-}$ AV cushion compared to non-diabetic *Notch1*$^{+/-}$ control (Figure 3B,D). Similar to the AV cushion size and cellular density data, we find a high degree of variability in the matDM-exposed WT littermates and as a result no statistical significance is reached between matDM-exposed WT and non-diabetic controls in either the Alcian blue staining or DPEAAE expression. Overall, these results indicate that GxE between *Notch1* haploinsufficiency and maternal diabetes impairs AV cushion morphogenesis potentially via disruption of ECM organization.

NOTCH1 haploinsufficiency acts synergistically with oxidative stress to dysregulate genes involved in EndMT and endocardial cushion morphogenesis

Previously published research from us and others have proposed matDM-associated oxidative stress as the key driver of cardiac maldevelopment, leading to increased incidence of CHD. To determine if there is elevated oxidative stress in matDM-exposed *Notch1*$^{+/-}$ embryos compared to non-diabetic controls, we probed E11.5 matDM-exposed and non-diabetic WT and *Notch1*$^{+/-}$ embryonic hearts with an antibody against 4-hydroxynoneal (4-HNE), a stable by-product of lipid peroxidation and a robust biomarker for cellular oxidative stress (48). We detected increased 4-HNE labeling in matDM-exposed *Notch1*$^{+/-}$ and WT littermates compared to non-diabetic controls while no difference was detected between *Notch1*$^{+/-}$ and WT matDM-exposed hearts, including in the AV cushions suggesting there are comparable levels of oxidative stress in matDM-exposed WT and *Notch1*$^{+/-}$ littermates at this timepoint (Supplemental Figure 3A, C). Increased oxidative stress can induce cellular apoptosis in diabetic embryos, particularly during the neurulation stage at E8.75 (49,50). To probe for increased apoptosis in matDM-exposed WT and *Notch1*$^{+/-}$ embryonic hearts, we performed TUNEL assay on E11.5 matDM-exposed and non-diabetic *Notch1*$^{+/-}$ and WT embryonic hearts. However, no significant differences were observed across groups, suggesting there is no increase in apoptosis in matDM-exposed cardiac tissues in either *Notch1*$^{+/-}$ or WT embryos at this time point (Supplemental Figure 3B,D).

To determine the molecular mechanisms underlying GxE between endothelial *Notch1* and matDM-associated oxidative stress, we utilized *NOTCH1*^{WT} and isogenic *NOTCH1*$^{+/-}$ (*NOTCH1* haploinsufficient) iPSC lines, generated as previously described (51,52). We differentiated *NOTCH1*^{WT} and *NOTCH1*$^{+/-}$ iPSC to endothelial cells (iEC) using previously published differentiation protocol (53). Following differentiation, subsets

of *NOTCH1*^{WT} and *NOTCH1*$^{+/-}$ iEC were either exposed to oxidative stress (50 µM H_2O_2) or left untreated as control, to mimic matDM-associated oxidative stress *in vitro.* After 4 days, total RNA was isolated from each iEC subset and bulk RNA sequencing performed for differential gene expression analysis. Principal component analysis of the sequenced samples revealed distinct clustering of biological replicates (n=3 per genotype/condition) with the largest variance observed between *NOTCH1*$^{+/-}$ and *NOTCH1*^{WT} in oxidative stress (Figure 4A). As expected, we observed high variance between *NOTCH1*$^{+/-}$ and *NOTCH1*^{WT} control samples, suggesting there are intrinsic transcriptomic differences between *NOTCH1*$^{+/-}$ and *NOTCH1*^{WT} iEC at baseline untreated condition. Differential gene expression analysis revealed there were 965 genes significantly differentially expressed (FDR adjusted p value <0.05, absolute $\log_2$ fold change > 0.75) between *NOTCH1*$^{+/-}$ and *NOTCH1*^{WT} iEC in control condition (437 upregulated and 528 downregulated) (Figure 4B, Extended Table 1). Next, we turned our attention to how these genotypes differed with respect to each other during exposure to oxidative stress. Differential gene expression analysis revealed there were 2890 genes significantly differentially expressed (FDR adjusted p value <0.05, absolute $\log_2$ fold change > 0.75) between *NOTCH1*$^{+/-}$ and *NOTCH1*^{WT} iEC under oxidative stress (1508 upregulated and 1382 downregulated) (Figure 4C, Extended Table 2). We confirmed ~40% downregulation of *Notch1* mRNA in *NOTCH1*$^{+/-}$ iEC under both conditions ($\log_2$ fold change = -0.64, FDR adjusted p value < 0.05 in control; $\log_2$ fold change = -0.61, FDR adjusted p value < 0.05 in oxidative stress), however, it was not assigned as DEG due to our stringent $\log_2$ fold change cutoff of 0.75. Comparison of DEG from control and oxidative stress revealed 638 genes were dysregulated in *NOTCH1*$^{+/-}$ iEC in both control

and oxidative stress while 2252 genes were dysregulated in *NOTCH1*$^{+/-}$ iEC only under oxidative stress (Figure 4D). Overrepresentation analysis of DEG in *NOTCH1*$^{+/-}$ iEC under each condition was performed. Top significant biological processes in *NOTCH1*$^{+/-}$ iEC in control condition included embryonic organ development, skeletal system morphogenesis and extracellular structure organization (Figure 4E, Extended Table 3). In contrast, top dysregulated biological processes in *NOTCH1*$^{+/-}$ in oxidative stress included terms related to cell division (*MKI67, MYBL2, CDC20, PLK1, CCNB1*), mesenchyme development (*APLNR, EFNB1*) and extracellular matrix organization (*COL1A1, COL11A1, MMP2*) (Figure 4F). While several biological pathways were commonly dysregulated in *NOTCH1*$^{+/-}$ iEC in both control and oxidative stress, including GO terms 'mesenchyme development', 'connective tissue development', 'collagen metabolic processes', 'proteoglycan metabolic processes', the number of DEG in each process was higher in *NOTCH1*$^{+/-}$ iEC in oxidative stress compared to control condition (Figure 4G). Additionally, many biological processes were found to be dysregulated in *NOTCH1*$^{+/-}$ iEC in oxidative stress including the terms 'nuclear division', 'mitotic sister chromatid segregation', 'extracellular matrix organization', 'heart morphogenesis', 'notch signaling', 'nitric oxide signaling pathway' among others (Figure 4G). Considering that extracellular matrix organization and proteoglycan metabolic processes are highly relevant processes in the context of endocardial cushion morphogenesis, we investigated the effect of oxidative stress in *NOTCH1*$^{+/-}$ iEC on genes within these terms, reporting several interconnected genes to be dysregulated across both processes (Figure H, I). Among DEG affecting extracellular matrix organization, majority were upregulated and many of these genes are known to be negative regulators of ECM organization (*DPP4, FAP, ANTXR1, CST3,*

EMILIN1) while majority of genes in proteoglycan metabolic process was downregulated (*BMPR1B, IGF1, COL11A1*). Taken together, these results suggest *Notch1* haploinsufficiency acts synergistically with oxidative stress to dysregulate gene regulatory networks crucial for endocardial cushion morphogenesis.

Overexpression of antioxidant gene, SOD1, does not reduce incidence of maternal diabetes-associated congenital heart disease in the setting of Notch1 haploinsufficiency

Oxidative stress is characterized by an imbalance of reactive oxygen species (ROS) production and antioxidant defense response. Superoxide dismutases (SOD) are crucial for neutralizing superoxide radicals, converting them to H_2O_2 which can be degraded to H_2O and O_2 by endogenous catalase and glutathione peroxidase. To determine if a genetic antioxidant strategy via overexpression of SOD1 is effective in rescuing CHD in a *Notch1* haploinsufficient background, we bred SOD1 overexpressing transgenic male mice (*SOD1*$^{+}$) to diabetic *Notch1*$^{+/-}$ females to generate WT, *Notch1*$^{+/-}$, *SOD1*$^{+}$ and *SOD1*$^{+}$*;Notch1*$^{+/-}$ compound mutant embryos (n=11 litters) (Figure 5A). We performed histological analysis of E14.5 embryonic hearts and found a significantly decreased incidence of VSD in *SOD1*$^{+}$ (1/25) compared to WT (6/23, Fisher's exact test p value = 0.044) (Figure 5B-D). This is consistent with prior publications showing overexpression of SOD1 in embryonic hearts can reduce the incidence of matDM-associated CHD in a WT setting (31, 32). However, no significant reduction in the incidence of VSD was noted when comparing *Notch1*$^{+/-}$ (12/19) and *SOD1*$^{+}$*;Notch1*$^{+/-}$ embryos (10/17, Fisher's exact test p value = 0.99). To account for litter variability, we used binomial regression with litter as a random effect to further analyze these results,

and while statistical significance was not achieved, a similar trend was noted (see Supporting Data Values). We compared the level of oxidative stress via 4-HNE labeling between the above genotypes and found decreased immunostaining of 4-HNE in *SOD1*$^{+}$ compared to WT while no difference was observed between the *Notch1*$^{+/-}$ and *SOD1*+*; Notch1*$^{+/-}$ (Supplemental figure 4A,B), suggesting *SOD1* overexpression cannot reduce oxidative stress in a *Notch1* haploinsufficient background. The failure of *SOD1* overexpression to reduce the incidence of VSD resulting from the *Notch1*-matDM interaction is consistent with our *in vitro* results showing an exacerbated effect on cardiac developmental process in *NOTCH1*$^{+/-}$ iEC exposed to H_2O_2. Overall, our results solidify the role of *Notch1* haploinsufficiency as a genetic modifier in maternal diabetes-associated CHD, highlighting the presence of gene-environment interactions and their mechanisms in CHD pathogenesis.

Discussion

Maternal diabetes mellitus (matDM) is an established risk factor for CHD; however, its effect on genetic susceptibilities has not been well described. In this study, we show matDM interacts with *Notch1* haploinsufficiency *in viv*o to increase the disease penetrance of a membranous VSD phenotype. We find that this GxE acts within the developing endothelial/endocardial and endocardial-derived cells and that *Notch1* haploinsufficiency sensitizes the effects of matDM on EndMT and AV cushion morphogenesis, affecting deposition of ECM components including versican. Using a human iPSC-based model, we demonstrate that oxidative stress exposed *NOTCH1*$^{+/-}$ endothelial cells have exacerbated effect on cardiac developmental processes compared

to oxidative stress exposed *NOTCH1*^{WT} iEC. We show effects of oxidative stress and *NOTCH1* haploinsufficiency converge to dysregulate networks underlying endocardial cushion morphogenesis. Finally, we find that targeting matDM-associated oxidative stress via overexpression of *SOD1* is unable to rescue VSD in a *Notch1* haploinsufficient background as compared to successful rescue in WT littermates. Taken together, these results reveal that susceptible genetic variation acts in combination with effects of matDM to disrupt cardiac development and increase the incidence of CHD.

Complex inheritance patterns and incomplete penetrance of CHD are often explained by genetic heterogeneity among individuals, with strong speculation as to the requirement of specific gene-environment or gene-gene interaction for disease manifestation (6,54). In humans, pathogenic *NOTCH1* variants are associated with a spectrum of CHD with variable expressivity (33-35). The Notch signaling pathway is highly conserved and *Notch1* heterozygosity in mice has been reported to interact with both environmental factors (e.g., gestational hypoxia, maternal diabetes) as well as genetic factors (e.g., deletion of *Nos3*) to increase the incidence of heart defects (27,55,56). Hence, *NOTCH1* variation may play a crucial role in multifactorial cases of CHD and results from this study corroborate the role of *NOTCH1* as both a genetic modifier and driver in CHD pathogenesis.

During cardiac development, activated NOTCH1 (N1CD*)* is expressed in the developing endocardium lining the AV canal and outflow tract; in synchrony with myocardial BMP signaling, N1CD coordinates initiation of EndMT and mesenchyme development at these regions to form the endocardial cushions (37,57). EndMT-derived

mesenchymal cells communicate with adjacent endocardial and myocardial layers to dynamically regulate organization and stratification of the ECM to form the valvuloseptal complex (24,25). Based on our *in vivo* results, matDM-exposed *Notch1*$^{+/-}$ endocardial cushions do not show any overt signs of initial EndMT failure as lineage tracing does not show a reduction in number of EndMT derived cells in either matDM-exposed WT or *Notch1*$^{+/-}$ littermates compared to non-diabetic controls. Instead, our results suggest that disruption in AV cushion formation results in smaller overall size of the AV cushion in matDM-exposed *Notch1*$^{+/-}$ with altered ECM deposition, specifically deposition of cleaved versican. This is consistent with recent reports that have revealed a requirement of N1CD to induce secretion of extracellular matrix remodeling and structural proteins within the developing AV cushion (58). Versican is essential for ventricular septum formation, and mice harboring mutant *Versican* exhibit smaller AV cushions and VSD (59). In comparison, matDM-exposed WT littermates displayed great variability in their AV cushion size, cell density and proteoglycan deposition, with only a subset trending similar to matDM exposed *Notch1*$^{+/-}$ animals, consistent with the low penetrance of disease observed in these animals. In addition, our *in vitro* findings revealed dysregulation of *BMP2* and *MMP2* expression in *NOTCH1*$^{+/-}$ iEC in oxidative stress. While Notch signaling is known to modulate expression of *MMP2*, required for proteolytic cleavage of versican, matDM has also been independently linked to decreased MMP2 expression in the AV cushions (28,60). Endocardial BMP2 has also been shown to be essential for later AV cushion morphogenesis, regulating deposition of ECM components such as *Col9a1*, *Has2, Postn,* and *Vcan* (61). Our results suggest *Notch1* haploinsufficiency can sensitize

the genetic network underlying ECM organization during AV cushion development with exposure to maternal diabetes-associated oxidative stress.

Although diabetes mellitus is characterized by chronic hyperglycemia, diabetic embryopathy is likely driven by a combination of metabolic imbalances occurring within the intrauterine diabetic milieu. Diabetes mellitus is associated with disruption of several metabolic pathways including glycolysis, sorbitol production, ketone formation, and increased synthesis of advanced glycation end-products, all of which result in increased ROS production and cellular oxidative stress (62-64). As expected, matDM-exposed *Notch1*$^{+/-}$ embryos exhibit oxidative stress comparable to matDM-exposed WT littermates, as shown by 4-HNE labeling. Antioxidant therapy has been tested by several research groups, including us, in an attempt to decrease the incidence of matDM-associated CHD but lack of consensus on route of administration and/ or strategy (genetic vs. pharmacologic) have led to inconsistent results (27,32,65). In this study, we find *SOD1* overexpression can only decrease the incidence of VSD in a WT background and cannot rescue VSD in a *Notch1* haploinsufficient setting. Based on 4-HNE labeling across matDM-exposed littermates, this seems to be due to inability of SOD1 to effectively reduce ROS levels below the required threshold for rescue in matDM-exposed *Notch1*$^{+/-}$ mice. Based on our *in vitro* studies, processes such as cell division and apoptosis were among the top significantly affected pathways in *NOTCH1* haploinsufficient iEC exposed in H_2O_2 along with ECM organization. Proliferation and apoptosis of mesenchymal cells within the endocardial cushions is carefully coordinated with the start of ECM stratification (66). Previous studies have shown increased apoptosis and decreased proliferation in embryonic hearts exposed to maternal diabetes, particularly at later stages of endocardial

cushion development. However, we did not find increased TUNEL+ apoptotic cells in matDM-exposed WT and *Notch1*$^{+/-}$ compared to non-diabetic controls, possibly due to small sample size and timing during embryonic development. Our *in vitro* results show decreased expression of *BMP4* specifically in *NOTCH1*$^{+/-}$ iEC exposed to H_2O_2 and BMP4 has been reported to mediate regulation of endocardial cushion apoptosis (30,67). As such, we speculate that a combination of dysregulated ROS-Notch signaling contributes to the magnified effect on cell division and cell death in *NOTCH1* haploinsufficiency and may be acting synergistically to cause VSD *in vivo*, thus making it unable to be rescued by *SOD1* overexpression alone.

Results from the *in vitro* experiments demonstrated relevant transcriptomic changes related endocardial cushion morphogenesis in *NOTCH1*$^{+/-}$ compared to *NOTCH1*^{WT} iEC in control condition, although they were not as affected as found in oxidative stress conditions. This supports the notion that a genetic hit in *NOTCH1* can "prime" the cell to a secondary environmental hit. Although *Notch1*$^{+/-}$ mice are not reported to have a congenital cardiac phenotype, they are known to have impaired lipid metabolism and develop aortic aneurysms with age (68,69). The lack of CHD in non-diabetic *Notch1*$^{+/-}$ mice may be explained by compensatory mechanisms occurring *in vivo* that cannot be recapitulated in our *in vitro* endothelial cell-autonomous system.

In summary, our work uncovers a composite effect of genetic variation and exposure to an environmental teratogen on cardiac morphogenesis. We report that these effects can disrupt specific cardiac developmental networks in a cell lineage-specific manner. Furthermore, we have shown that broad therapeutic strategies, such as the use

of antioxidants, may not be effective in genetically sensitized populations. Future studies should aim to uncover other potential gene-environment interactions that may be contributing to matDM-associated CHD. Studies of this nature will pave the way for personalized therapy to improve outcomes from diabetic pregnancies in genetically susceptible individuals and reduce the risk of maternal DM-associated CHD.

Limitations of the study

In this study, we defined diabetic mice as those having fasting blood glucose greater than >200 mg/dL. However, we were not able to monitor or control blood glucose levels throughout pregnancy and attribute a degree of variability in the matDM-exposed samples due to differences in maternal glucose levels. We have performed binomial regression analysis with litter as a random factor to increase confidence in our results. In this study, we used C57BL/6J mice for all *in vivo* studies. However, strain-related differences may lead to variable phenotypic results. In the context of gene-environment, it is important to determine whether *Notch1* haploinsufficiency in a different strain/genetic background can also interact with maternal diabetes mellitus to increase CHD incidence. Consequently, we focused on the effect of GxE in AV cushion development as our phenotype was limited to membranous ventricular septal defects and we found no significant difference in OFT cushions. Future studies with other animal strains may identify additional cardiac phenotypes that may require investigation into other cardiac developmental processes. Additionally, we focused on endothelial/ endocardial and endocardial-derived cell specific GxE as *Notch1* expression is enriched in this cell lineage. However, NOTCH1 can also play a role during cardiomyocyte differentiation and specification and investigation of the non-endothelial roles of *Notch1* in the context of maternal diabetes mellitus is beyond the

scope of this paper and will be reserved for future investigations. For our *in vitro* studies, all experiments were conducted using iPSC lines derived from a single healthy donor. Whether similar results will be observed with multiple donor cell lines is yet to be determined.

Methods

Sex as a biological variable

Our study did not consider sex to be a biological variable as our studies involved evaluation of embryonic hearts.

Experimental mouse models

WT C57BL/6 (Jax, #000664), *Rosa26*^{mTmG} (Jax, #007676), *Tie2-Cre*$^{+}$ (Jax, #004128), and *SOD1-tg* (Jax, #002297) animals were purchased from Jackson Laboratory. *Notch1*$^{+/-}$ and *Notch1*$^{fl/fl}$ mice were generated and genotyped as described previously (70,71). *Rosa*$^{+/+}$*; Notch1*$^{+/-}$ compound mutants were generated by intercrossing *Rosa26*^{mTmG} with *Notch1*$^{+/-}$ mice. Six to eight week old female *WT, Notch1*$^{fl/fl}$, *Rosa*$^{+/+}$*; Notch1*$^{+/-}$, and *Notch1*$^{+/-}$ mice were used to induce diabetes mellitus by intraperitoneal injection of STZ (NC0146241, Fisher Scientific) dissolved in 0.01 mol/L citrate buffer, pH 4.5 at 75 mg/kg body weight for 3 consecutive days. Two weeks after STZ injection, mice were fasted for 8 hours during the light cycle, and glucose levels were measured using the AlphaTrak 2 veterinary blood glucometer calibrated specifically for rodents from tail vein blood (Abbott Laboratories). Mice with fasting blood glucose ≥200 mg/dL (11 mmol/L) were defined as diabetic and used for timed breeding and embryo collections.

Mouse embryo collection

Timed mating was performed using the following pairs: non-diabetic *Notch1*$^{+/-}$ males and diabetic WT females, non-diabetic *Tie2-Cre*$^{+}$ males with diabetic and non-diabetic *Notch1*$^{fl/fl}$ females or diabetic and non-diabetic *Rosa*$^{+/+}$*; Notch1*$^{+/-}$, and non-diabetic *SOD1-tg* males with diabetic *Notch1*$^{+/-}$ females. Mice were maintained on a 12-hour-light/dark cycle, with noon of the day of vaginal plug observation defined as E0.5. Pregnant dams were euthanized using isoflurane and embryos were collected at E11.5 and E14.5.

Embryo processing and histological analysis

Harvested embryos were fixed in 4% paraformaldehyde at 4°C overnight followed by alcohol gradient dehydration and paraffin embedding. Serial tissue sections (6 µm) of the embryonic heart were collected for histological analysis. H&E staining (Vector Laboratories) was used to visualize gross morphology and Alcian blue staining (Vector Laboratories) to visualize proteoglycan deposition. Images were taken using Keyence BZ-X810 Fluorescence Microscope.

Amira3D reconstruction of developing endocardial cushions and cell counts

Serial sections of embryonic hearts from diabetic and non-diabetic group were imaged at 10x magnification using Olympus BX51 and images were loaded onto Amira3D v2023.2 for alignment and segmentation of AV endocardial cushions. Volume measurement was recorded using the MaterialStatistics module. To count endMT derived cells within the AV cushion, diabetic and non-diabetic E11.5 *Rosa*^{mTmG}*; WT; Tie2-Cre*$^{+}$

and *Rosa*^{mTmG}*; Notch1*$^{+/-}$*; Tie2-Cre*$^{+}$ sections were used. Following immunostaining against GFP, the number of cells in the AV cushion was quantified by counting nuclei stained with DAPI of GFP+ cells within defined area of the AV cushion. At least three readings were taken from each image and three serial sections were used for each biological replicate to obtain mean cell count/ area within the AV cushion.

Immunofluorescence and immunohistochemistry

Histological sections of embryonic hearts were deparaffinized using xylene and gradient ethanol washes, followed by antigen retrieval using heat mediated citrate-based Antigen Unmasking solution (H-3300, Vector laboratories). For immunofluorescence, tissue sections were blocked with 2% normal horse serum in 1X phosphate buffer saline with 0.1% Tween-20 (PBST) for 1 hour and then incubated with rabbit anti-GFP (Abcam #ab290, 1:200), and rabbit anti-DPEAE (Invitrogen #PA1-1748A, 1:100) overnight at 4°C. Following 1X PBST wash, sections were incubated with donkey anti-rabbit secondary antibody conjugated to Alexa Fluor 488 for 1 hour at room temperature in the dark (Invitrogen # A-21206). Sections were washed 3 times with 1X PBST, and counterstained with VECTASHIELD Vibrance Mounting Medium with DAPI. Fluorescent images were visualized using the Keyence BZX-810 Fluorescence Microscope. Relative fluorescence intensity was measured using ImageJ software. For immunohistochemistry, unmasked tissue sections were incubated in 3% H_2O_2 followed by blocking in 1% bovine serum albumin in 1X PBST for 1 hour and then incubated with mouse anti-4-HNE (R&D systems #MAB3249, 1:100) overnight at 4°C. Following 1X PBST wash, sections were incubated with SignalStain Boost IHC detection reagent (HRP-anti-mouse; Cell Signaling

Technology #8125) for 1 hour at room temperature. SignalStain DAB substrate kit (Cell Signaling Technology #8059) was used to develop the stain. Images were taken using the Keyence BZX-810 Microscope in bright field. Mean gray value of each image was measured using ImageJ software.

Cellular apoptosis

TUNEL assay was performed to detect cellular apoptosis using TUNEL Assay Kit (Cell Signaling Technology #64936S) according to manufacturer's instructions. For nuclear staining, slides were mounted using VECTASHIELD Vibrance Mounting Medium with DAPI. Fluorescent images were taken using Keyence BZX-810 Fluorescence Microscope and percent of TUNEL+ cells within the embryonic heart and were counted using ImageJ software.

Culture of iPSC and directed differentiation into endothelial lineage and oxidative stress treatments

NOTCH1^{WT} and *NOTCH1*$^{+/-}$ iPSC were generated as previously described (51, 52). For differentiation into endothelial cells, *NOTCH1*^{WT} and *NOTCH1*$^{+/-}$ iPSC were cultured in complete E8 media until ~90% confluency and then changed to differentiation media following published protocol (53). For oxidative stress studies, H_2O_2 was added to EGM2 media at a final concentration of 50 µM and cells were exposed for 4 days, with media refreshment every 24 hours.

RNAseq analysis

Following oxidative stress treatment for 4 days, total RNA was collected from *NOTCH1*^{WT} and *NOTCH1*$^{+/-}$ iEC using Total RNA Purification Kit (Norgen Biotek) according to manufacturer's instructions. RNA was prepared for sequencing following provider's instructions (Novogene Corporation) and sequenced on an NovaSeq 6000 (Illumina). Primary processing and expression quantification of the reads were performed by DataPrudence (A Carboctet Brand). FASTQ files were trimmed to remove Illumina adaptor sequences and low-quality reads using TrimGalore! in "paired" mode (72). Paired, trimmed reads were then aligned against Homo sapiens assembly version GRCh38.p14, GENCODE 44 (http://Jul2023.archive.ensembl.org/Homo_sapiens/Info/Annotation), using the STAR alignment tool (v2.7.10b) with "--quantMode TranscriptomeSAM" option (73). The transcriptome-aligned BAM was used to collect gene-level and transcriptome-level count estimates using RSEM (v1.3.1) (74). The gene count estimates were used to identify differentially expressed genes using DESeq2 (v1.34.0) (75). Overrepresentation analysis was performed using R package, genekitr (https://CRAN.R-project.org/package=genekitr) and cross-validated with clusterProfiler (76). GO terms were simplified using GO semantic similarity analysis using in-built GOsim() function in genekitr (77). Volcano plots were created using ggplot2 (78). Gene regulatory networks were visualized and annotated using Cytoscape (79).

Data availability

Values for all data points shown in graphs are reported in the supporting data values files. The RNAseq data produced in this study were depositeyed to the NCBI's GEO database (accession no. GSE279323). Additional information is available upon request.

Statistical analysis

Categorical data are presented with count and percent while continuous data are presented as mean and standard deviation (SD). Our experiments included embryos from multiple diabetic dams and introduces the possibility that correlation of outcomes from embryos from the same litter could impact results. For binomial outcomes (incidence of VSD in Figures 2 and 7), Fisher's exact test was used and binomial regression models with robust standard errors accounting for litter were conducted as sensitivity analyses (Supporting Data Values). For continuous outcomes, linear regression with random effects for litter were conducted and t-tests for the estimated marginal means for all pairwise comparisons were carried out using Tukey's correction to adjust for multiple testing. A p value less than 0.05 was considered statistically significant.

Study approval

All animal use was approved and monitored on protocol AR09-00056 by the Institutional Animal Care and Use Committee at the Research Institute at Nationwide Children's Hospital and conducted in accordance with the NIH's *Guide for the Care and Use of Laboratory Animals*.

Author contributions

VG and TZC conceived the study and experimental design with input from DL and M-TZ. TZC and SCG performed and analyzed the experiments. The murine studies were performed by TZC, SCG, HBG, and EMC. MZ generated and provided iPSC lines. Bioinformatics analyses were performed by TZC, ASR and YB. Statistical analysis was performed by TZC, SC and VG. TZC and VG wrote the manuscript with input from all authors.

Acknowledgements

The authors acknowledge funding support from NIH/NHLBI (R01HL144009) to V.G. and (T32HL166149) to A.R. We thank members of the Biomorphology Core at Nationwide Children's Hospital for histology support as well as S. Adamczak, C. Boettcher and the Animal Resource Core at Nationwide Children's Hospital for animal support. We would also like to acknowledge Dr. T. Vetter in the Microscopy Core at Nationwide Children's Hospital for imaging support. We thank Dr. S. Manivannan, Novogene Corporation and Carboctet LLC for RNA sequencing and bioinformatics analysis support. The authors would like to acknowledge Dr. D. Lewandowski for manuscript editing assistance. We would like to acknowledge all members in the laboratories of Dr. V. Garg, Dr. D. Li, Dr. M-T Zhao, and Dr. J. Jang for technical support.

References

1. Tsao CW, et al. Heart disease and stroke statistics—2022 update: a report from the American Heart Association. *Circulation*. 2022;145(8):e153-e639.

2. Jin SC, et al. Contribution of rare inherited and de novo variants in 2,871 congenital heart disease probands. *Nat Genet*. 2017;49(11):1593-1601.

3. Sifrim A, et al. Distinct genetic architectures for syndromic and nonsyndromic congenital heart defects identified by exome sequencing. *Nat Genet*. 2016;48(9):1060-1065.

4. Morton SU, et al. Genomic frontiers in congenital heart disease. *Nat Rev Cardiol*. 2022;19(1):26-42.

5. Yasuhara J, Garg V. Genetics of congenital heart disease: a narrative review of recent advances and clinical implications. *Transl Pediatr*. 2021;10(9):2366.

6. Nora JJ. Multifactorial inheritance hypothesis for the etiology of congenital heart diseases: the genetic-environmental interaction. *Circulation*. 1968;38(3):604-617.

7. Vecoli C, et al. Congenital heart disease: the crossroads of genetics, epigenetics and environment. *Curr Genomics*. 2014;15(5):390-399.

8. Simeone RM, et al. Proportion of selected congenital heart defects attributable to recognized risk factors. *Annals Epidemiol*. 2016;26(12):838-845.

9. Kalisch-Smith JI, et al. Environmental risk factors for congenital heart disease. *Cold Spring Harb Perspect Biol*. 2020;12(3):a037234.

10. Loffredo CA, et al. Maternal diabetes: an independent risk factor for major cardiovascular malformations with increased mortality of affected infants. *Teratology*. 2001;64(2):98-106.

11. Helle EI, et al. First trimester plasma glucose values in women without diabetes are associated with risk for congenital heart disease in offspring. *J Pediatr*. 2018;195:275-278.

12. Hoang TT, et al. Original findings and updated meta-analysis for the association between maternal diabetes and risk for congenital heart disease phenotypes. *Am J Epidemiol*. 2017;186(1):118-128.

13. Øyen N, et al. Prepregnancy diabetes and offspring risk of congenital heart disease: a nationwide cohort study. *Circulation*. 2016;133(23):2243-2253.

14. Choudhury TZ, et al. Impact of maternal hyperglycemia on cardiac development: Insights from animal models. *Genesis*. 2021;59(11):e23449.

15. Nishino T, et al. Single-cell multimodal analyses reveal epigenomic and transcriptomic basis for birth defects in maternal diabetes. *Nat Cardiovasc Res*. 2023;2(12):1190-1203.

16. Manivannan S, et al. Single-cell transcriptomic profiling unveils dysregulation of cardiac progenitor cells and cardiomyocytes in a mouse model of maternal hyperglycemia. *Commun Biol*. 2022;5(1):820.

17. Rowland TW, et al. Congenital heart disease in infants of diabetic mothers. *J Pediatr*. 1973;83(5):815-820.

18. Correa A. Pregestational diabetes mellitus and congenital heart defects. *Am Heart Assoc;* 2016. p. 2219-2221.

19. Christoffels V, Jensen B. Cardiac morphogenesis: specification of the four-chambered heart. *Cold Spring Harb Perspect Biol*. 2020;12(10):a037143.

20. Meilhac SM, Buckingham ME. The deployment of cell lineages that form the mammalian heart. *Nat Rev Cardiol*. 2018;15(11):705-724.

21. Kinsella MG, Fitzharris TP. Origin of cushion tissue in the developing chick heart: cinematographic recordings of in situ formation. *Science*. 1980;207(4437):1359-1360.

22. Mjaatvedt CH, Markwald RR. Induction of an epithelial-mesenchymal transition by an in vivo adheron-like complex. *Dev Biol*. 1989;136(1):118-128.

23. Markwald RR, et al. Structural development of endocardial cushions. *Am J Anat*. 1977;148(1):85-119.

24. Wessels A, et al. The development of the atrioventricular junction in the human heart. *Circ Res*. 1996;78(1):110-117.

25. Webb S, et al. Formation of the atrioventricular septal structures in the normal mouse. *Circ Res*. 1998;82(6):645-656.

26. Kirby ML, Waldo KL. Neural crest and cardiovascular patterning. *Circ Res*. 1995;77(2):211-215.

27. Basu M, et al. Epigenetic mechanisms underlying maternal diabetes-associated risk of congenital heart disease. *JCI Insight*. 2017;2(20)

28. Enciso JM, et al. Elevated glucose inhibits VEGF-A–mediated endocardial cushion formation: modulation by PECAM-1 and MMP-2. *J Cell Biol*. 2003;160(4):605-615.

29. Cao S, et al. Restoring BMP4 expression in vascular endothelial progenitors ameliorates maternal diabetes-induced apoptosis and neural tube defects. *Cell Death Dis*. 2020;11(10):859.

30. Kumar SD, et al. Maternal diabetes induces congenital heart defects in mice by altering the expression of genes involved in cardiovascular development. *Cardiovasc Diabetol*. 2007;6:1-14.

31. Wang F, et al. Oxidative stress is responsible for maternal diabetes-impaired transforming growth factor beta signaling in the developing mouse heart. *Am J Obstet Gynecol*. 2015;212(5):650. e1-650. e11.

32. Wang F, et al. Superoxide dismutase 1 in vivo ameliorates maternal diabetes mellitus–induced apoptosis and heart defects through restoration of impaired Wnt signaling. *Circulation Cardiovasc Genet*. 2015;8(5):665-676.

33. Garg V, et al. Mutations in NOTCH1 cause aortic valve disease. *Nature*. 2005;437(7056):270-274.

34. McBride KL, et al. NOTCH1 mutations in individuals with left ventricular outflow tract malformations reduce ligand-induced signaling. *Human Mol Genet*. 2008;17(18):2886-2893.

35. Kerstjens-Frederikse et al. Cardiovascular malformations caused by NOTCH1 mutations do not keep left: data on 428 probands with left-sided CHD and their families. *Genet Med*. 2016;18(9):914-923.

36. Meester JA, et al. Overlapping but distinct roles for NOTCH receptors in human cardiovascular disease. *Clin Genet*. 2019;95(1):85-94.

37. Timmerman LA, et al. Notch promotes epithelial-mesenchymal transition during cardiac development and oncogenic transformation. *Genes Dev*. 2004;18(1):99-115.

38. de la Pompa JL, Epstein JA. Coordinating tissue interactions: Notch signaling in cardiac development and disease. *Dev Cell*. 2012;22(2):244-254.

39. Del Monte G, et al. Monitoring Notch1 activity in development: evidence for a feedback regulatory loop. *Dev Dyn*. 2007;236(9):2594-2614.

40. Grego-Bessa J, et al. Notch signaling is essential for ventricular chamber development. *Dev Cell*. 2007;12(3):415-429.

41. Golub MS, Sobin CA. Statistical modeling with litter as a random effect in mixed models to manage “intralitter likeness”. *Neurotoxicol Teratol*. 2020;77:106841.

42. Greenland S, et al. Statistical tests, P values, confidence intervals, and power: a guide to misinterpretations. *Eur J Epidemiol*. 2016;31(4):337-350.

43. Gittenberger-de Groot AC, et al. Morphogenesis and molecular considerations on congenital cardiac septal defects. *Ann Med*. 2014;46(8):640-652.

44. Camenisch TD, et al. Regulation of cardiac cushion development by hyaluronan. *Exp Clin Cardiol*. 2001;6(1):4.

45. Mjaatvedt C, et al. TheCspg2Gene, disrupted in thehdfMutant, is required for right cardiac chamber and endocardial cushion formation. *Dev Biol*. 1998;202(1):56-66.

46. Deepe R, et al. The mesenchymal cap of the atrial septum and atrial and atrioventricular septation. *J Cardiovasc Dev Dis*. 2020;7(4):50.

47. Kern CB, et al. Proteolytic cleavage of versican during cardiac cushion morphogenesis. *Dev Dyn*. 2006;235(8):2238-2247.

48. Jinsmaa Y, et al. Products of oxidative stress inhibit aldehyde oxidation and reduction pathways in dopamine catabolism yielding elevated levels of a reactive intermediate. *Chem Res Toxicol*. 2009;22(5):835-841.

49. Dong D, et al. Maternal diabetes triggers DNA damage and DNA damage response in neurulation stage embryos through oxidative stress. *Biochem Biophys Res Commun*. 2015;467(2):407-412.

50. Li X, et al. Oxidative stress–induced JNK1/2 activation triggers proapoptotic signaling and apoptosis that leads to diabetic embryopathy. *Diabetes*. 2012;61(8):2084-2092.

51. Ye S, et al. Impaired human cardiac cell development due to NOTCH1 deficiency. *Circ Res*. 2023;132(2):187-204.

52. Aljuhani M, et al. Generation and characterization of a human induced pluripotent stem cell line heterozygous for a NOTCH1 mutation (NCHi014-A). *Stem Cell Res*. 2024;74:103281.

53. Joachim A, et al. Generation of cardiomyocytes and endothelial cells from human iPSCs by chemical modulation of Wnt signaling. *Induced Pluripotent Stem Cells and Human Disease: Methods and Protocols*. Springer; 2021:335-344.

54. Zhu H, et al. Importance of gene–environment interactions in the etiology of selected birth defects. *Clin Genet*. 2009;75(5):409-423.

55. Bosse K, et al. Endothelial nitric oxide signaling regulates Notch1 in aortic valve disease. *J Mol Cell Cardiol*. 2013;60:27-35.

56. Chapman G, et al. Functional genomics and gene-environment interaction highlight the complexity of congenital heart disease caused by Notch pathway variants. *Hum Mol Genet*. 2020;29(4):566-579.

57. Luxán G, et al. Endocardial Notch signaling in cardiac development and disease. *Circ Res*. 2016;118(1):e1-e18.

58. Torregrosa-Carrion R, et al. NOTCH Activation Promotes Valve Formation by Regulating the Endocardial Secretome*[S]. *Mol Cell Proteomics*. 2019;18(9):1782-1795.

59. Hatano S, et al. Versican/PG-M is essential for ventricular septal formation subsequent to cardiac atrioventricular cushion development. *Glycobiology*. 2012;22(9):1268-1277.

60. Fischer A, et al. Combined loss of Hey1 and HeyL causes congenital heart defects because of impaired epithelial to mesenchymal transition. *Circ Res*. 2007;100(6):856-863.

61. Saxon JG, et al. BMP2 expression in the endocardial lineage is required for AV endocardial cushion maturation and remodeling. *Dev Biol*. 2017;430(1):113-128.

62. Perez-Ramirez CA, et al. Atlas of fetal metabolism during mid-to-late gestation and diabetic pregnancy. *Cell*. 2024;187(1):204-215. e14.

63. Ramos-Riera KP, et al. Oxidative stress: A common imbalance in diabetes and epilepsy. *Metab Brain Dis*. 2023;38(3):767-782.

64. Yan Lj. Redox imbalance stress in diabetes mellitus: Role of the polyol pathway. *Animal Mod Exp Med*. 2018;1(1):7-13.

65. Moazzen H, et al. N-Acetylcysteine prevents congenital heart defects induced by pregestational diabetes. *Cardiovasc Diabetol*. 2014;13:1-13.

66. Rabkin E, et al. Activated interstitial myofibroblasts express catabolic enzymes and mediate matrix remodeling in myxomatous heart valves. *Circulation*. 2001;104(21):2525-2532.

67. Zhao Z, Rivkees SA. Programmed cell death in the developing heart: regulation by BMP4 and FGF2. *Dev Dyn*. 2000;217(4):388-400.

68. Yamaguchi K, et al. Notch1 haploinsufficiency in mice accelerates adipogenesis. *Sci Rep*. 2021;11(1):16761.

69. Koenig SN, et al. Notch1 haploinsufficiency causes ascending aortic aneurysms in mice. *JCI insight*. 2017;2(21)

70. Conlon RA, et al. Notch1 is required for the coordinate segmentation of somites. *Development*. 1995;121(5):1533-1545.

71. Radtke F, et al. Deficient T cell fate specification in mice with an induced inactivation of Notch1. *Immunity*. 1999;10(5):547-558.

72. Krueger F, et al. FelixKrueger/TrimGalore: v0. 6.10-add default decompression path (0.6. 10). Zenodo. 2023.

73. Dobin A, et al. STAR: ultrafast universal RNA-seq aligner. *Bioinformatics*. 2013;29(1):15-21.

74. Li B, Dewey CN. RSEM: accurate transcript quantification from RNA-Seq data with or without a reference genome. *BMC bioinformatics*. 2011;12:1-16.

75. Love Ml, et al. Moderated estimation of fold change and dispersion for RNA-seq data with DESeq2. *Genome Biol*. 2014;15:1-21.

76. Wu T, et al. clusterProfiler 4.0: A universal enrichment tool for interpreting omics data. *Innovation (Camb)*. 2021;2(3)

77. Resnik P. Semantic similarity in a taxonomy: An information-based measure and its application to problems of ambiguity in natural language. *J Artif Intell Res*. 1999;11:95-130.

78. Wilkinson L. ggplot2: elegant graphics for data analysis by WICKHAM, H. Oxford University Press; 2011.

79. Shannon P, et al. Cytoscape: a software environment for integrated models of biomolecular interaction networks. *Genome Res*. 2003;13(11):2498-2504.

Figure Legends

Figure 1. Endothelial/endocardial haploinsufficiency of *Notch1* is sufficient for gene-environment interaction with maternal diabetes mellitus. (A) Breeding scheme to generate diabetic and non-diabetic E14.5 *Notch1*$^{fl/wt}$ and *Notch1*$^{fl/wt}$*;Tie2-Cre*$^{+}$ for histological analysis. (B) Table showing incidence of VSD in E14.5 embryos. (C) Representative images of matDM-exposed and non-diabetic *Notch1*$^{fl/wt}$ and *Notch1*$^{fl/wt}$*;Tie2-Cre*$^{+}$ embryonic hearts. Asterisk denotes VSD. ND, Non-diabetic; DM, diabetic; RA, right atrium; LA, left atrium; RV, right ventricle; LV, left ventricle; IVS, interventricular septum; VSD, ventricular septal defect. P value obtained from Fisher's exact test; scale bar = 200 μm.

Figure 2. Maternal diabetes mellitus impairs atrioventricular cushion size in *Notch1* haploinsufficient embryonic hearts. (A) Three-dimensional (3D) projection of AV cushions in E11.5 control and matDM-exposed WT and *Notch1*$^{+/-}$ embryonic hearts. Top panel shows overlay of 3D projection on corresponding 2D transverse section of the heart; scale bar = 100 μm. Bottom panel shows AV cushion 3D projections rotated 90 degrees to show AV cushion span right to left across AV canal. (B) Quantification of AV cushion volume from 3D projections. (C) Control and matDM-exposed WT and *Notch1*$^{+/-}$ embryonic hearts showing Tie2-Cre driven Rosa$^{mT;mG}$ based GFP expression. GFP+ cells in the heart represent all endocardial and endocardial derived cells. Top panel shows GFP expression throughout the embryonic heart; Scale bar = 200 μm. Bottom panel shows representative zoomed in images of AV cushions for each genotype. (D) Quantification of GFP+ cell nuclei within AV cushion based on DAPI staining. Each point

represents a single animal of corresponding genotype/condition. P values obtained from t-tests for the estimated marginal means for all pairwise comparisons using Tukey's correction to adjust for multiple testing. AV, atrioventricular; dor, dorsal; R, right; L, left; ven, ventral.

Figure 3. Maternal diabetes mellitus impairs proteoglycan distribution within atrioventricular cushion of *Notch1* haploinsufficient embryonic hearts. (A) Alcian blue staining of control and matDM-exposed E11.5 WT and *Notch1*$^{+/-}$ AV cushion. (B) Immunostaining of cleaved Versican (DPEAAE) in control and matDM-exposed WT and *Notch1*$^{+/-}$ AV cushion. (C) Quantification of alcian blue staining from (A). (D) Quantification of DPEAAE staining from (B). Each point represents a single animal of corresponding genotype/condition. AV, atrioventricular; p values obtained from t-tests for the estimated marginal means for all pairwise comparisons using Tukey's correction to adjust for multiple testing. Scale bar = 100 µm.

Figure 4. *NOTCH1* haploinsufficiency and oxidative stress act synergistically to dysregulate processes involved in endocardial cushion morphogenesis. (A) Principal component analysis (PCA) shows the grouping of biological replicates and high variance between genotype and response to oxidative stress treatment. (B) Volcano plot showing upregulated and downregulated DEG in *NOTCH1*$^{+/-}$ vs *NOTCH1*^{WT} iEC in control condition. (C) Volcano plot showing upregulated and downregulated DEG in *NOTCH1*$^{+/-}$ *and NOTCH1*^{WT} iEC in oxidative stress. (D) Venn diagram showing number of common and unique DEG in *NOTCH1*$^{+/-}$ iEC vs *NOTCH1*^{WT} in control and oxidative stress condition followed by heatmap showing top 50 significant DEG in *NOTCH1*$^{+/-}$ vs *NOTCH1*^{WT} in

control and oxidative stress condition. (E) Top significantly enriched GO BP terms in *NOTCH1*$^{+/-}$ iEC vs *NOTCH1*^{WT} in control. (F) Top significantly enriched GO BP terms in *NOTCH1*$^{+/-}$ iEC vs *NOTCH1*^{WT} in oxidative stress. (G) Heatmap of dysregulated pathways in *NOTCH1*$^{+/-}$ vs *NOTCH1*^{WT} in control and oxidative stress. (H) DEG in in *NOTCH1*$^{+/-}$ iEC vs *NOTCH1*^{WT} in oxidative stress that affect GO term 'extracellular matrix organization'. Asterisk indicates genes that were also dysregulated in *NOTCH1*$^{+/-}$ iEC vs *NOTCH1*^{WT} in control. (I) DEG in in *NOTCH1*$^{+/-}$ iEC vs *NOTCH1*^{WT} in oxidative stress that affect GO term 'proteoglycan metabolic processes. Asterisk indicates genes that are also significantly differentially expressed in *NOTCH1*$^{+/-}$ iEC vs *NOTCH1*^{WT} in control. DEG, differentially expressed genes; FC, fold change; GO, gene ontology; BP, biological processes; Padj, False discovery rate adjusted p value.

Figure 5. *SOD1* overexpression does not rescue maternal diabetes mellitus-associated VSD in the setting of *Notch1* haploinsufficiency. (A) Breeding scheme to generate E14.5 DM WT*, SOD1*$^{+}$*, Notch1*$^{+/-}$*, Notch1*$^{+/-}$*;SOD1*$^{+}$ embryos (B, C) Graph and table showing incidence of VSD in E14.5 embryos by genotype. (D) Representative images of matDM-exposed WT*, SOD1*$^{+}$*, Notch1*$^{+/-}$*, and Notch1*$^{+/-}$*;SOD1*$^{+}$ embryonic hearts. Asterisk denotes VSD. RA, right atrium; LA, left atrium; RV, right ventricle; LV, left ventricle; IVS, interventricular septum; VSD, ventricular septal defect; DM, diabetic; *p*-values obtained from Fisher's exact test; scale bar = 200 μm.

Supplemental Figure 1. Gene-environment interaction between maternal diabetes mellitus and *Notch1* haploinsufficiency increases penetrance of ventricular septal defects. (A) Breeding scheme to generate E14.5 WT and *Notch1*$^{+/-}$ embryos for

histological analysis. (B) Table showing incidence of VSD in E14.5 embryos. (C) Representative images of matDM-exposed WT and *Notch1*$^{+/-}$ embryonic hearts. Asterisk denotes VSD. ND, Non-diabetic; DM, diabetic; RA, right atrium; LA, left atrium; RV, right ventricle; LV, left ventricle; IVS, interventricular septum; VSD, ventricular septal defect. *p*-values obtained from Fisher's exact test; scale bar = 200 μm.

Supplemental Figure 2. Gene-environment interaction between maternal diabetes mellitus and *Notch1* haploinsufficiency does not affect endocardial cushions of the outflow tract. (A) Three-dimensional (3D) projection of OFT cushions in E11.5 control and matDM-exposed WT and *Notch1*$^{+/-}$ embryonic hearts. Top panel shows overlay of 3D projection on corresponding 2D transverse section of the heart; scale bar = 100 μm. (B) Quantification of OFT cushion volume from 3D projections. Each point represents a single animal of corresponding genotype/condition. P values obtained from t-tests for the estimated marginal means for all pairwise comparisons using Tukey's correction to adjust for multiple testing; OFT, outflow tract.

Supplemental Figure 3. Oxidative stress and cellular apoptosis in WT and *Notch1*$^{+/-}$ embryonic hearts exposed to maternal diabetes mellitus. (A) Immunostaining against 4-HNE in control and matDM-exposed WT and *Notch1*$^{+/-}$ at E11.5. (B) TUNEL assay of control and matDM-exposed WT and *Notch1*$^{+/-}$ at E11.5. White arrows indicate TUNEL+ cells (C) Quantification of (A). (D) Quantification of (B). Each dot represents single animal of corresponding genotype/condition. WT, wildtype; ND, non-diabetic; DM, diabetic; p values obtained from t-tests for the estimated marginal means for all pairwise comparisons using Tukey's correction to adjust for multiple testing.

Supplemental Figure 4. Oxidative stress can be modulated by SOD1 overexpression. (A) Immunostaining of 4-HNE in E14.5 matDM-exposed WT, *SOD1*$^{+}$, *Notch1*$^{+/-}$, *Notch1*$^{+/-}$*;SOD1*$^{+}$ embryonic hearts (B) Quantification of (A). Each dot represents single animal of corresponding genotype. WT, wildtype; DM, exposed to maternal diabetes; p values obtained from t-tests for the estimated marginal means for all pairwise comparisons using Tukey's correction to adjust for multiple testing. Scale bar = 200 µm.

Figures

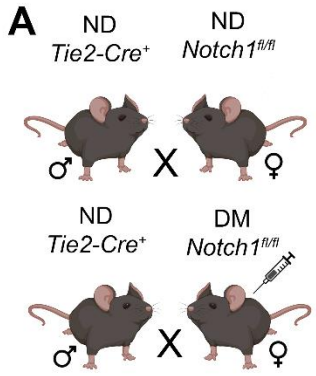

B

Maternal environment	Genotype	VSD incidence (%)	p value
Control	*Notch1*$^{fl/wt}$	0/11 (0%)	-
	Notch1$^{fl/wt}$;*Tie2-Cre*$^{+}$	0/12 (0%)	
MatDM	*Notch1*$^{fl/wt}$	3/31 (9.7%)	0.02
	Notch1$^{fl/wt}$;*Tie2-Cre*$^{+}$	7/17 (41%)	

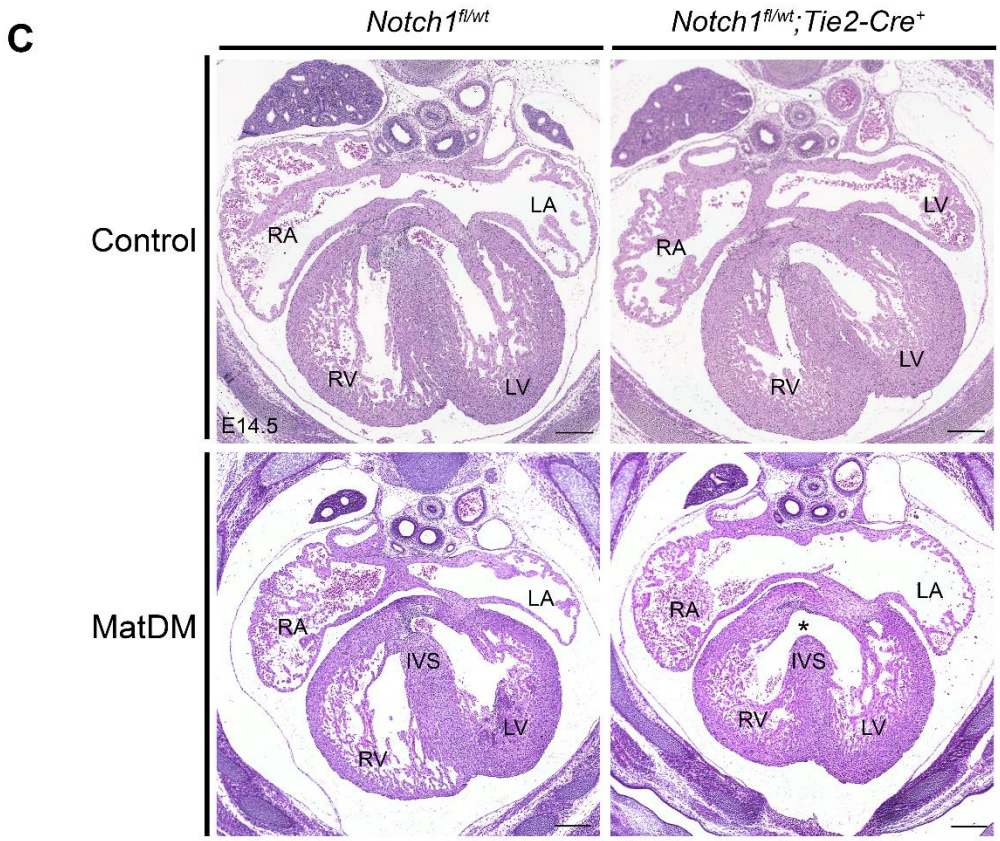

Figure 1. Endothelial/endocardial haploinsufficiency of *Notch1* is sufficient for gene-environment interaction with maternal diabetes mellitus. (A) Breeding scheme to generate diabetic and non-diabetic E14.5 *Notch1*$^{fl/wt}$ and *Notch1*$^{fl/wt}$;*Tie2-Cre*$^{+}$ for histological analysis. (B) Table showing incidence of VSD in E14.5 embryos. (C) Representative images of matDM-exposed and non-diabetic *Notch1*$^{fl/wt}$ and *Notch1*$^{fl/wt}$;*Tie2-Cre*$^{+}$ embryonic hearts. Asterisk denotes VSD. ND, Non-diabetic; DM, diabetic; RA, right atrium; LA, left atrium; RV, right ventricle; LV, left ventricle; IVS, interventricular septum; VSD, ventricular septal defect. P value obtained from Fisher's exact test; scale bar = 200 µm.

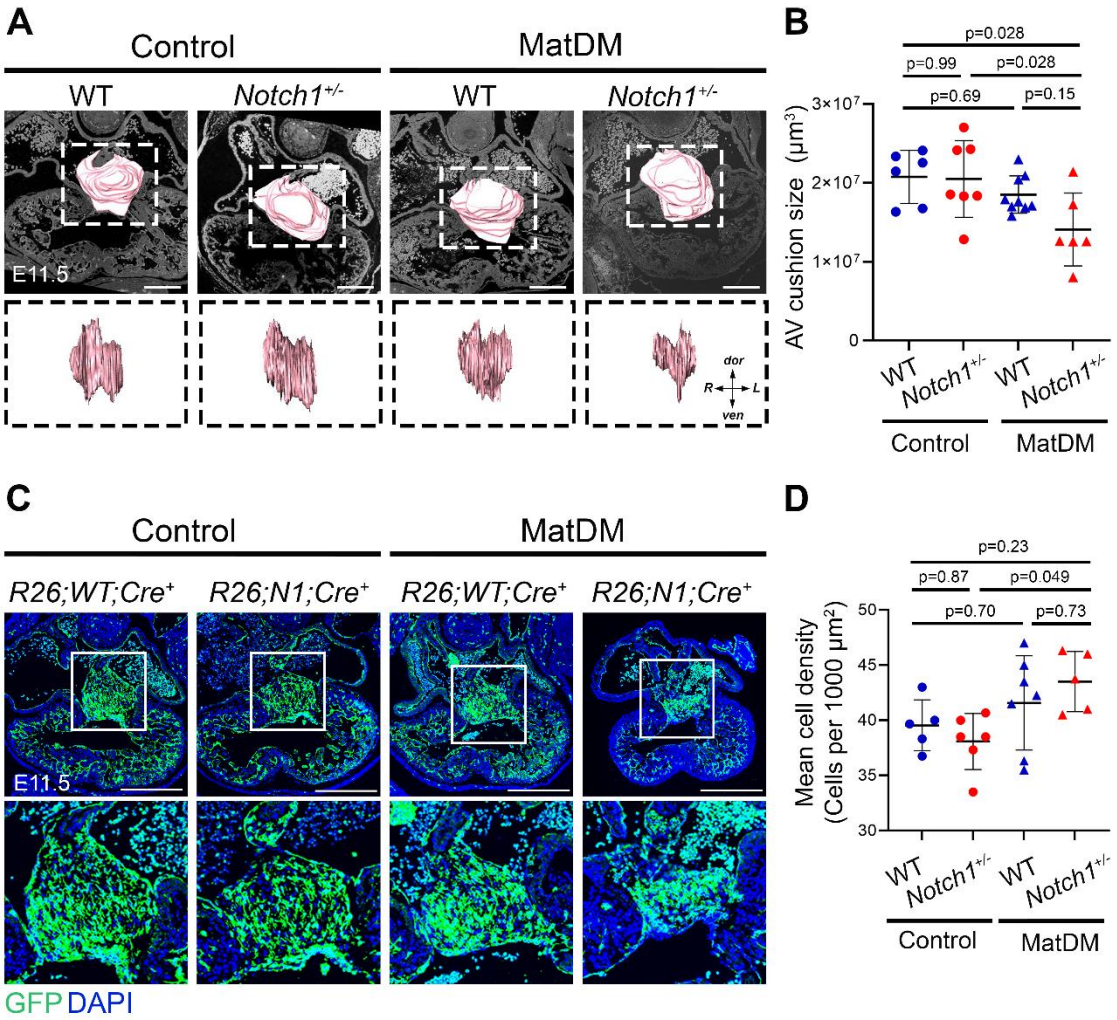

Figure 2. Maternal diabetes mellitus impairs atrioventricular cushion size in *Notch1* haploinsufficient embryonic hearts. (A) Three-dimensional (3D) projection of AV cushions in E11.5 control and matDM-exposed WT and *Notch1*$^{+/-}$ embryonic hearts. Top panel shows overlay of 3D projection on corresponding 2D transverse section of the heart; scale bar = 100 µm. Bottom panel shows AV cushion 3D projections rotated 90 degrees to show AV cushion span right to left across AV canal. (B) Quantification of AV cushion volume from 3D projections. (C) Control and matDM-exposed WT and *Notch1*$^{+/-}$ embryonic hearts showing Tie2-Cre driven Rosa$^{mT;mG}$ based GFP expression. GFP+ cells in the heart represent all endocardial and endocardial derived cells. Top panel shows GFP expression throughout the embryonic heart; Scale bar = 200 µm. Bottom panel shows representative zoomed in images of AV cushions for each genotype. (D) Quantification of GFP+ cell nuclei within AV cushion based on DAPI staining. Each point represents a single animal of corresponding genotype/condition. P values obtained from t-tests for the estimated marginal means for all pairwise comparisons using Tukey's correction to adjust for multiple testing. AV, atrioventricular; dor, dorsal; R, right; L, left; ven, ventral.

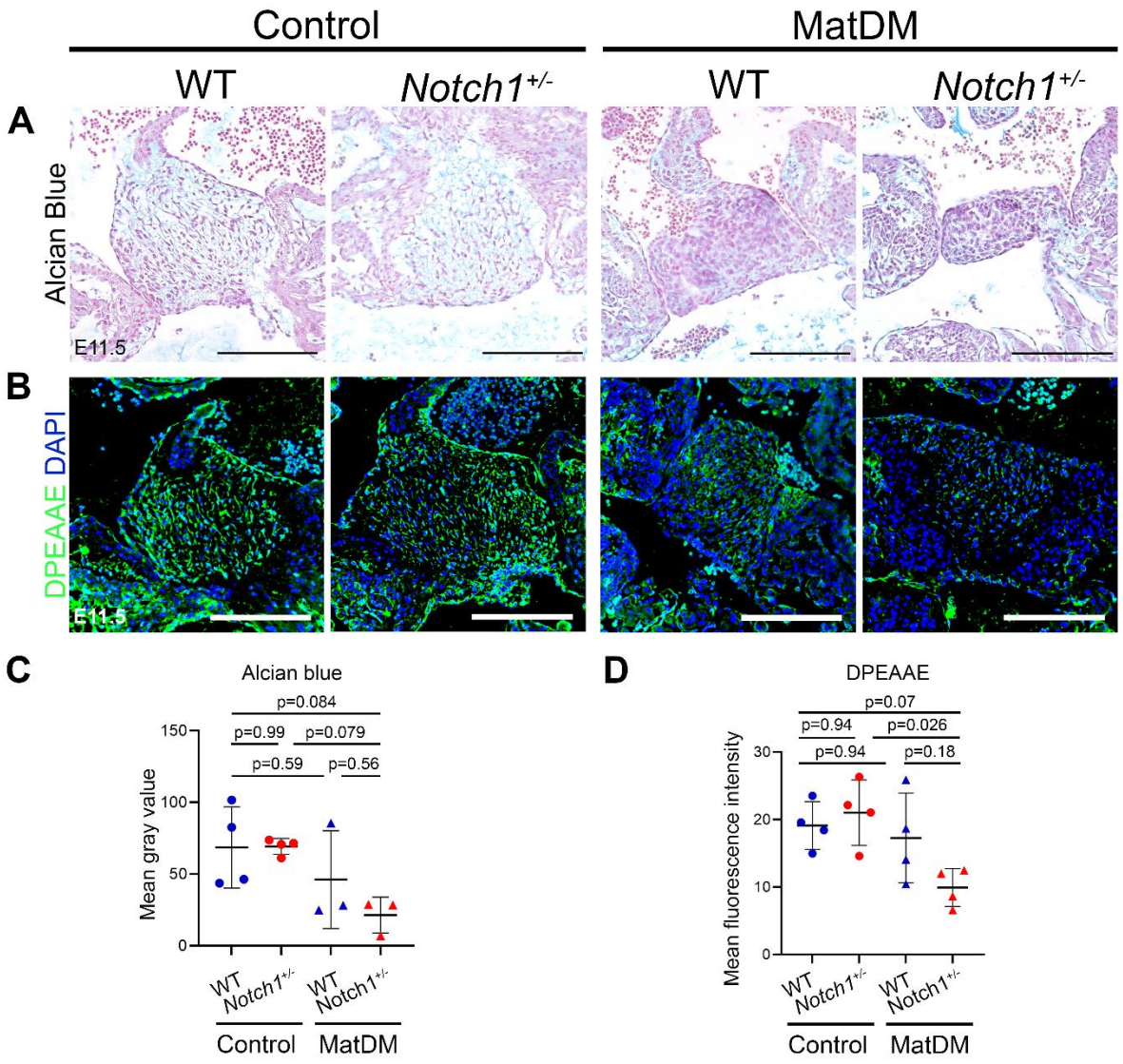

Figure 3. Maternal diabetes mellitus impairs proteoglycan distribution within atrioventricular cushion of *Notch1* haploinsufficient embryonic hearts. (A) Alcian blue staining of control and matDM-exposed E11.5 WT and *Notch1*$^{+/-}$ AV cushion. (B) Immunostaining of cleaved Versican (DPEAAE) in control and matDM-exposed WT and *Notch1*$^{+/-}$ AV cushion. (C) Quantification of alcian blue staining from (A). (D) Quantification of DPEAAE staining from (B). Each point represents a single animal of corresponding genotype/condition. AV, atrioventricular; p values obtained from t-tests for the estimated marginal means for all pairwise comparisons using Tukey's correction to adjust for multiple testing. Scale bar = 100 µm.

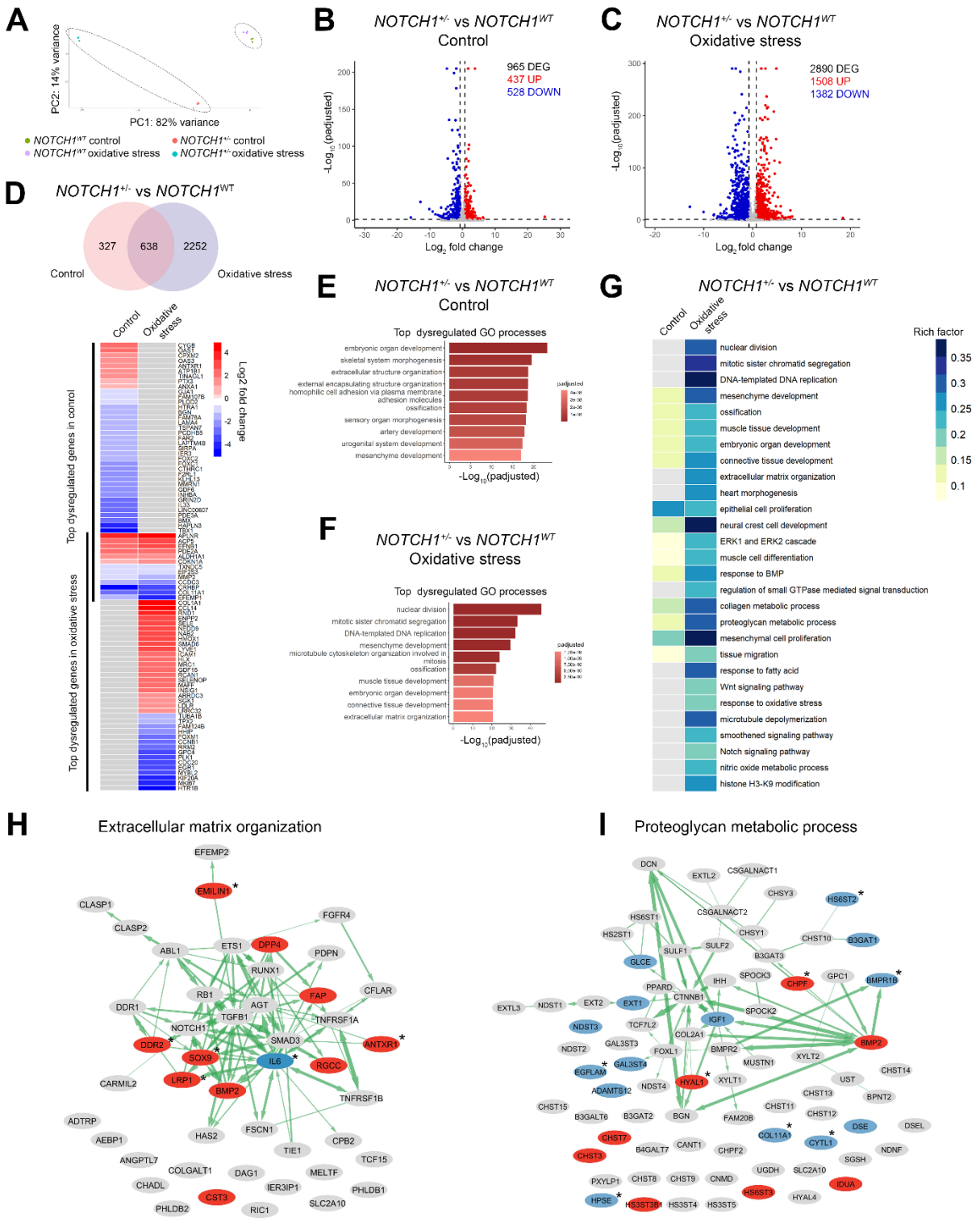
A
PC2: 14% variance
PC1: 82% variance
NOTCH1WT control
NOTCH1+/- control
NOTCH1WT oxidative stress
NOTCH1+/- oxidative stress
B
NOTCH1+/- vs NOTCH1WT
Control
965 DEG
437 UP
528 DOWN
-Log10(padjusted)
Log2 fold change
C
NOTCH1+/- vs NOTCH1WT
Oxidative stress
2890 DEG
1508 UP
1382 DOWN
-Log10(padjusted)
Log2 fold change
D
NOTCH1+/- vs NOTCH1WT
327
638
2252
Control
Oxidative stress
Control
Oxidative stress
Top dysregulated genes in control
Top dysregulated genes in oxidative stress
Log2 fold change
E
NOTCH1+/- vs NOTCH1WT
Control
Top dysregulated GO processes
embryonic organ development
skeletal system morphogenesis
extracellular structure organization
external encapsulating structure organization
homophilic cell adhesion via plasma membrane adhesion molecules
ossification
sensory organ morphogenesis
artery development
urogenital system development
mesenchyme development
padjusted
-Log10(padjusted)
F
NOTCH1+/- vs NOTCH1WT
Oxidative stress
Top dysregulated GO processes
nuclear division
mitotic sister chromatid segregation
DNA-templated DNA replication
mesenchyme development
microtubule cytoskeleton organization involved in mitosis
ossification
muscle tissue development
embryonic organ development
connective tissue development
extracellular matrix organization
padjusted
-Log10(padjusted)
G
NOTCH1+/- vs NOTCH1WT
Control
Oxidative stress
Rich factor
0.35
0.3
0.25
0.2
0.15
0.1
nuclear division
mitotic sister chromatid segregation
DNA-templated DNA replication
mesenchyme development
ossification
muscle tissue development
embryonic organ development
connective tissue development
extracellular matrix organization
heart morphogenesis
epithelial cell proliferation
neural crest cell development
ERK1 and ERK2 cascade
muscle cell differentiation
response to BMP
regulation of small GTPase mediated signal transduction
collagen metabolic process
proteoglycan metabolic process
mesenchymal cell proliferation
tissue migration
response to fatty acid
Wnt signaling pathway
response to oxidative stress
microtubule depolymerization
smoothened signaling pathway
Notch signaling pathway
nitric oxide metabolic process
histone H3-K9 modification
H
Extracellular matrix organization
EFEMP2
EMILIN1
CLASP1
CLASP2
FGFR4
ABL1
ETS1
DPP4
PDPN
RUNX1
RB1
FAP
CFLAR
DDR1
AGT
TGFB1
TNFRSF1A
NOTCH1
DDR2
SMAD3
ANTXR1
SOX9
IL6
RGCC
CARMIL2
LRP1
BMP2
TNFRSF1B
ADTRP
AEBP1
HAS2
FSCN1
CPB2
TIE1
TCF15
ANGPTL7
COLGALT1
DAG1
MELTF
CHADL
IER3IP1
PHLDB1
CST3
PHLDB2
RIC1
SLC2A10
I
Proteoglycan metabolic process
DCN
EXTL2
CSGALNACT1
CHSY3
HS6ST2
CSGALNACT2
HS6ST1
HS2ST1
CHSY1
CHST10
B3GAT1
SULF1
SULF2
B3GAT3
GLCE
SPOCK3
CHPF
GPC1
BMPR1B
PPARD
IHH
CTNNB1
EXTL3
NDST1
EXT2
EXT1
SPOCK2
IGF1
NDST3
TCF7L2
COL2A1
NDST2
GAL3ST3
FOXL1
BMPR2
BMP2
XYLT2
EGFLAM
GAL3ST4
MUSTN1
CHST14
HYAL1
XYLT1
UST
ADAMTS12
NDST4
CHST13
BPNT2
CHST15
CHST11
B3GALT6
B3GAT2
BGN
FAM20B
CHST12
DSE
DSEL
CHST7
COL11A1
CYTL1
B4GALT7
CANT1
CHPF2
NDNF
CHST3
SGSH
PXYLP1
CHST8
CHST9
CNMD
UGDH
SLC2A10
IDUA
HS6ST3
HPSE
HS3ST3B1
HS3ST4
HS3ST5
HYAL4

Figure 4. *NOTCH1* haploinsufficiency and oxidative stress act synergistically to dysregulate processes involved in endocardial cushion morphogenesis. (A) Principal component analysis (PCA) shows the grouping of biological replicates and high variance between genotype and response to oxidative stress treatment. (B) Volcano plot showing upregulated and downregulated DEG in *NOTCH1*$^{+/-}$ vs *NOTCH1*^{WT} iEC in control condition. (C) Volcano plot showing upregulated and downregulated DEG in *NOTCH1*$^{+/-}$ *and NOTCH1*^{WT} iEC in oxidative stress. (D) Venn diagram showing number of common and unique DEG in *NOTCH1*$^{+/-}$ iEC vs *NOTCH1*^{WT} in control and oxidative stress condition followed by heatmap showing top 50 significant DEG in *NOTCH1*$^{+/-}$ vs *NOTCH1*^{WT} in control and oxidative stress condition. (E) Top significantly enriched GO BP terms in *NOTCH1*$^{+/-}$ iEC vs *NOTCH1*^{WT} in control. (F) Top significantly enriched GO BP terms in *NOTCH1*$^{+/-}$ iEC vs *NOTCH1*^{WT} in oxidative stress. (G) Heatmap of dysregulated pathways in *NOTCH1*$^{+/-}$ vs *NOTCH1*^{WT} in control and oxidative stress. (H) DEG in in *NOTCH1*$^{+/-}$ iEC vs *NOTCH1*^{WT} in oxidative stress that affect GO term 'extracellular matrix organization'. Asterisk indicates genes that were also dysregulated in *NOTCH1*$^{+/-}$ iEC vs *NOTCH1*^{WT} in control. (I) DEG in in *NOTCH1*$^{+/-}$ iEC vs *NOTCH1*^{WT} in oxidative stress that affect GO term 'proteoglycan metabolic processes. Asterisk indicates genes that are also significantly differentially expressed in *NOTCH1*$^{+/-}$ iEC vs *NOTCH1*^{WT} in control. DEG, differentially expressed genes; FC, fold change; GO, gene ontology; BP, biological processes; Padj, False discovery rate adjusted p value.

A

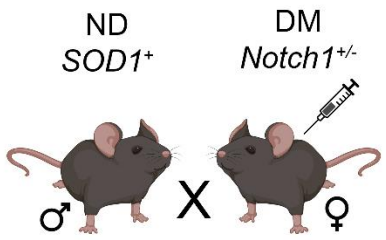

B

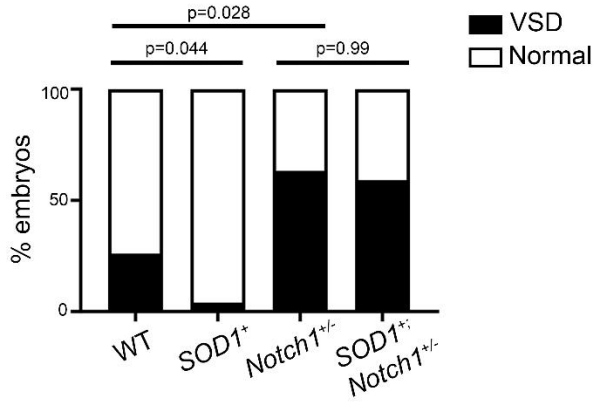

C

Genotype	Incidence of VSD (%)	p value
WT	6/23 (26%)	0.044
SOD1^{+}	1/25 (4%)	0.028
Notch1$^{+/-}$	12/19 (63%)	0.99
SOD1^{+}*; Notch1*$^{+/-}$	10/17 (58.8%)	

D

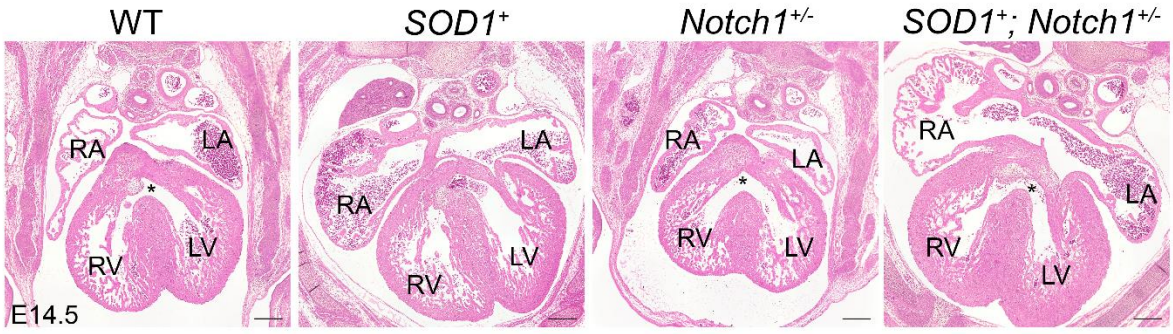

Figure 5. *SOD1* overexpression does not rescue maternal diabetes mellitus-associated VSD in the setting of *Notch1* haploinsufficiency. (A) Breeding scheme to generate E14.5 DM WT, *SOD1*$^{+}$, *Notch1*$^{+/-}$, *Notch1*$^{+/-}$*;SOD1*$^{+}$ embryos (B, C) Graph and table showing incidence of VSD in E14.5 embryos by genotype. (D) Representative images of matDM-exposed WT, *SOD1*$^{+}$, *Notch1*$^{+/-}$, *and Notch1*$^{+/-}$*;SOD1*$^{+}$ embryonic hearts. Asterisk denotes VSD. RA, right atrium; LA, left atrium; RV, right ventricle; LV, left ventricle; IVS, interventricular septum; VSD, ventricular septal defect; DM, diabetic; *p*-values obtained from Fisher's exact test; scale bar = 200 μm.